UTX inhibition suppresses proliferation and promotes apoptosis in patient-derived glioblastoma stem cells by modulating periostin expression

Yan Luan
Xi'an Jiaotong University
Yingfei Liu
Xi'an Jiaotong University
Jingwen Xue
Xi'an Jiaotong University
Ke Wang
Xi'an Jiaotong University
Kaige Ma
Xi'an Jiaotong University
Haixia Lu
Xi'an Jiaotong University
Xinlin Chen
Xi'an Jiaotong University
Yong Liu
Xi'an Jiaotong University
Zhichao Zhang
zhangzhichao@xjtu.edu.cn

Xi'an Jiaotong University https://orcid.org/0000-0001-7990-101X

Research Article

Keywords: UTX, Patient-derived glioblastoma stem cells, Periostin, Proliferation, Apoptosis

Posted Date: December 29th, 2022

DOI: https://doi.org/10.21203/rs.3.rs-2082131/v2

Version of Record: A version of this preprint was published at Journal of Cellular Physiology on January 12th, 2024. See the published version at https://doi.org/10.1002/jcp.31178.

Abstract

Glioblastoma stem cells (GSCs) link tightly to glioblastoma (GBM) development, progression, therapeutic resistance and recurrence, suggesting GSCs as a novel target for drug discovery. UTX, a histone H3K27 demethylase, participates in regulating multiple cancer types. However, less is known about the function of UTX in GBM, let alone in GSCs. Our study aims to investigate the role and regulatory mechanism of UTX on GSCs. TCGA data showed that higher UTX expression was found in GBM and inversely correlated with survival. UTX inhibition hindered GBM cell growth and caused cell apoptosis. Subsequently, we cultured the primary GSCs, which were isolated from three patients. UTX inhibition suppressed cell proliferation and promoted apoptosis in GSCs. RNA-seq was performed to analyze the gene expression changes after silencing UTX in GSCs. The results indicated that UTX-mediated genes were strongly correlated with GBM progression and regulatory tumor microenvironment (TME). Transwell co-cultured experiment showed that silencing UTX in the transwell chamber GSCs could also inhibit the well plate cell proliferation. Protein-protein interaction analysis revealed that periostin (POSTN) played a role in the UTX-mediated transcriptional regulatory network. Replenishment of POSTN abolished the effect of UTX inhibition on GSCs proliferation and apoptosis, ablated the differential expression of intra- and extracellular levels of COL1A1 and VCAM1. Combining the above results together, our study demonstrated that UTX inhibition hindered POSTN expression by enhancing the H3K27me2/3 level, eventually resulting in inhibiting proliferation and promoting apoptosis of patient-derived GSCs. Our findings may provide a novel and effective strategy for the treatment of GBM.

Introduction

As the most common primitive malignant brain tumor, Glioblastoma (GBM) is notorious for rapid progression, fast relapse and high metastasis [1]. Despite the great effort made in recent years, GBM treatment still remains unfavorable, and the 5-year survival rate for patients with GBM is only approximately 3–5% [2]. One of the major challenges in treating GBM is the extensive cellular heterogeneity, it contains a fraction of stem cell-like cancer cells called glioblastoma stem cells (GSCs). Accumulating evidence suggests that GSCs is mainly associated with tumor maintenance, recurrence, and therapeutic resistance [3, 4]. Therefore, GSCs has emerged as an attractive and novel therapeutic target for GBM.

The *Ubiquitously Transcribed Tetratricopeptide Repeat on chromosome X* (UTX, also called KDM6A) is a histone demethylase that catalyzes the removal of di- and tri-methyl marks at histone H3 lysine 27 (H3K27), which, in turn, regulates several types of stem cells such as embryonic stem cells (ESCs), induced pluripotent stem cells (iPSCs) and neural stem cells (NSCs) [5–7]. Besides having a direct role in regulating normal stem cells, UTX is also strongly associated with multiple types of cancer stem cells [8, 9]. Aberrant expression of UTX underpinned a substantial component of epigenetic deregulation, and it is an important factor in the development and progression of cancer. UTX deficiency increased cancer stem cells and caused bladder cancer in cooperation with p53 haploinsufficiency [10]. Pharmacological inhibition of UTX impairs chemotherapy-induced breast cancer stem cells enrichment and impairs tumor

initiation [11]. In contrast, overexpression of UTX promoted colorectal cancer stem cells proliferation and enrichment [12]. Although the exact role of UTX in GSCs is poorly understood at present, inhibition of JMJD3 (also called KDM6B, an H3K27me3 demethylase) suppressed glioma cell proliferation, migration, and promoted cell apoptosis [13]. These phenomena suggest UTX might involve in the regulation of GSCs. UTX affects the modulation of cell behavior through precisely regulated gene expression. However, the target gene by which UTX directly regulates expression is still not fully understood.

Cancer stem cells (CSCs) reside in niches, which are adjacent local tumor microenvironments. These niches regulate the CSCs proliferation, survival and tumorigenesis, maintain the pool of CSCs and protect them from the immune system [14]. As one of the components of the extracellular matrix, periostin (POSTN, also known as OSF-2) belongs to the fasciclin family and mediates communications between cells and their extracellular microenvironment. POSTN is secreted by different cell types in solid tumors and exerts its functions through establishing and remodeling the tumor microenvironment (TME) and CSCs niche [15, 16]. During the development of lung cancer, POSTN contributes to the CSCs maintenance and POSTN inhibition prevents metastasis [17]. Overexpression of POSTN enhances colorectal CSCs proliferation and promotes colorectal tumorigenesis and metastasis [18]. In GBM, POSTN similarly plays a pivotal role in tumor progression, recurrence and metastasis [19]. POSTN expression level was correlated with the malignancy of GBM and recurrence. Overexpression of POSTN promoted GBM cell adhesion and invasion [20]. More importantly, Silencing POSTN markedly inhibited tumor growth and impaired the survival of GSCs [21]. These results indicated that POSTN might be a key regulator of GSCs fates. However, it remains largely unclear whether and how POSTN expression is regulated is poorly understood.

In this study, we report that UTX is highly expressed in GBM tissue and inversely related to survival. UTX inhibition increased the methylation of H3K27 in the POSTN gene, thereby suppressing its expression which ultimately inhibits growth and tumorigenesis. These results may reveal new insight into the onset of gliomagenesis and progression, and provide a vigorous therapeutic strategy for GBM treatment.

Materials And Methods

Human glioma transcriptome analysis

RNA-sequencing expression profiles and corresponding clinical information for GBM and low-grade gliomas (LGG) were downloaded from the Cancer Genome Atlas (TCGA) Data Matrix portal (Level3, https://tcga-data.nci.nih.gov/tcga/dataAccessMatrix.htm). Statistical analysis and ggplot2 (v3.3.2) were completed using R program v4.0.3, Log2 (TPM+1) was calculated using the scaled estimated expression values of genes. *p*-value <0.05 was considered statistically significant. Kaplan–Meier survival curves were analyzed using the UCSC Xena browser (https://xenabrowser.net/).

Human glioma cell line culture

The LN229 cell line was purchased from American Type Culture Collection (ATCC, USA), and the U251 MG cell line was purchased from Procell (China). 3×10^5 cells were seeded in T25 flasks and incubated in an incubator (SANYO, Japan) with 5% CO2 and 95% air at 37 °C. The medium consisted of Dulbecco's Modified Eagle's Medium (DMEM), 10% fetal bovine serum (FBS), 100 U/mL penicillin and 100 μg/mL streptomycin (all from Gibco, USA). The cell subculture was trypsinized, mechanically blown to create single-cell suspension, and cryopreserved with a liquid nitrogen tank when necessary.

Patient-derive glioblastoma stem cells culture

Human glioblastoma stem cells (GSCs) were isolated from 3 post-surgical samples (GSC-02, GSC-05 and GSC-08). GSC-02 patient underwent surgery at the First Affiliated Hospital of Xi'an Jiaotong University; GSC-05 patient underwent surgery at the Second Affiliated Hospital of Xi'an Jiaotong University; GSC-08 patient underwent surgery at Shaanxi Provincial Peoples' Hospital. None of the patients received any treatment prior to the intervention. This study was performed in accordance with the principles of the Declaration of Helsinki. Clinical information and tumor samples were collected with informed consent. The detailed information was shown in Supplementary Table S1. Single GSCs were isolated as previously described and with minor modifications [22]. Briefly, after washing 3 times with cold DMEM/F12 (1:1) medium (Gibco), the GBM tissue was cut into small pieces and incubated with dissociation medium (200 μL Collagenase type I (10 mg / mL, Sigma), 200 μL Dispase II (20 mg / mL, Sigma) and 1.6 mL DMEM/F12 (1:1) medium) at 37 °C for 12 min. Then, the tissue was mechanically dissociated using a pipette and filtered using a 40 μm cell strainer (BD Falcon), followed by centrifugation at 1,000 rpm for 3 min. Cells were seeded at 4×10^5 cell/ml in non-adhesive T25 flasks with 5 mL complete medium, consisted of DMEM/F12 (1:1), 1% N2, 2% B27 (minus vitamin A), 20 ng/mL EGF, and 10 ng/mL bFGF. After culturing for 5-7 days, the formation of 80-200 μM sphere was observed. For single-cell adhesive culture, the sphere was dissociated into single cells using ACCUTASE™ (Stemcell Technologies, Canada) and plated in poly-D-lysine-coated 24-well plates.

UTX knockdown treatment

The small interfering RNA (siRNA) specific to human UTX and scrambled siRNA negative control (siNC) were synthesized by Genechem (Shanghai, China). The sequences were as follows:

si-UTX-1: 5'-AUUUCAGUGGGCUAUUAAATT-3',

si-UTX-2: 5'-ACGAAAUAUCAAGGUUUCATT-3',

si-UTX-3: 5'-CUAUGGAUGCUUUGCAAGCTT-3',

siNC: 5'-UUCUCCGAACGUGUCACGUTT-3'.

LN229 and U251 MG cells were grown on 24-well plates, and Lipofectamine 2000 reagent (Invitrogen) was used to deliver the siRNA (100 nM/well). The knockdown efficiency was evaluated by qRT-PCR and Western blot. The lentivirus vector containing shRNA targeting human UTX (shUTX) or negative control

vectors (shNC) was purchased from Genechem (Shanghai, China). Three lentivirus vectors were used in this study; one containing eGFP was used to measure transfection efficiency and orthotopic tumor formation assay, another which did not express fluorescent protein was used for the majority of the subsequent experiment, and the luciferase-expressing lentivirus was used for orthotopic glioblastoma experiments. Cells (2×10^4 cells/well) were seeded in a 24-well plate and infected with 2 μL KD-UTX (1×10^8 viruses, MOI = 1:10) or 1μl shNC (1×10^8 viruses, MOI = 1:5), respectively. One day later, the infected cells were selected with puromycin for 24 hours. For the GBM cells, the concentration of puromycin was 2.5 μg/ml, and 1.6 μg/ml of puromycin was used for GSCs.

Immunostaining

Cells were fixed with 4% paraformaldehyde (PFA) at room temperature for 20 min followed by washing three times with PBS. Then, cells were permeabilized in 0.1% Triton X-100 for 15 min and blocked with blocking buffer (containing 5% bovine serum albumin and 5% horse serum in PBS) for 1 h, followed by incubating with the primary antibodies overnight at 4°C. After washing three times with PBS, cells were then incubated with suitable secondary antibodies. The information of the first and secondary antibodies were shown in Supplementary Table S2. The negative control samples were just incubated in the blocking buffer instead of the primary antibody. Nuclei were visualized with DAPI-containing mounting medium (Vector, USA). Images were acquired using a fluorescence microscope equipped with a digital camera (BX51 + DP71, Olympus, Japan) and analyzed with ImageJ software (NIH, USA). The sphere-formation images were taken with a Leica SP8 confocal microscope equipped with a × 40 oil immersion lens.

BrdU incorporation

Following the treatment, GBM cells were incubated with 10 μg/mL of BrdU for 1 hour, and GSCs were treated with BrdU for 2 hours. The BrdU-labeled cells were further detected by immunostaining. To identify the BrdU-labeled cells, cells were pretreated with 2 N HCl for 30 min at 37°C, followed by neutralizing with 0.1 M borate buffer (pH8.5) for 15 min. The percentage of labeled cells was evaluated and normalized by the PI-stained nuclei or Sox2-positive cells.

TUNEL assay

The terminal deoxynucleotidyl transferase dUTP nick end labeling (TUNEL) assay was used for detecting cell apoptosis according to the manufacturer's instructions (Roche Diagnostics, USA). In brief, cells were fixed with 4% PFA for 30 min, followed by permeabilization using 0.1% Triton X-100 in 0.1% sodium citrate buffer for 2 min on ice. Then, cells were incubated with 50 μL TUNEL reaction mixture for 1 h at 37°C. After washing with PBS, nuclei were stained with DAPI-containing mounting medium (Vector). Images were acquired using a fluorescence microscope equipped with a 40× objective (BX51 + DP71, Olympus) and analyzed with Image-Pro Plus 5.0 software (Media Cybernetics, USA).

Flow cytometry analysis

For cell cycle analysis, the treated cells were dissociated with trypsin into single cells and fixed with pre-cooling 75% ethanol overnight at 4°C. After washing twice with PBS, cells were stained with propidium iodide solution (100 μg/mL, Sigma-Aldrich, USA) containing 100 μg/mL RNase A (New England Biolabs, USA) for 15 min at 37°C and away from light. The cell cycle analysis was performed using a FACSCalibur system (BD Biosciences, USA) with an excitation at 488 nm and emission at 630 nm. 1×10^5 cells were detected for each sample. The data were collected using the FACSortCellquect software (BD Biosciences), and the DNA content and cell cycle distribution were determined using the Modfit LT software (BD Biosciences). The proliferation index was used to evaluate the changes in the cell cycle distribution with the following formula: proliferation index = (S+G2/M) / (G0/G1+S+G2/M).

Apoptosis analysis was performed using the FITC Annexin V apoptosis detection kit (BD Biosciences, USA). After treatment, cells were dissociated into single cells, washed twice with pre-cooling PBS and resuspended in 1 × binding buffer. Then, 200 μL of the cell suspension (more than 1×10^5 cells) was transferred to a 5 mL FACS tube (BD Biosciences) and stained in duplicate with 10 μL of FITC Annexin V conjugate and 10 μL of propidium iodide (10 mg/mL) for 15 min in dark at room temperature. Apoptosis was analyzed using a FACSCalibur (BD Biosciences) with 488 nm excitation for Annexin V (emission collected at 530 nm) and 488 nm excitation for PI (emission collected at 630 nm). The data were collected with FACSort Cellquect software (BD Biosciences) and the percent of apoptotic cells was referred to the apoptotic index with the following formula: (LR+UR) / (UL+LL+LR+UR).

Colony formation assay

Cells (500 cells/well) were seeded into a six-well plate and cultured in normal conditions for 14 days. After fixation with 4% PFA, cells were stained with crystal violet solution. The number of colonies was counted for each sample and data were presented in samples from at least 3 independent experiments.

Western blot analysis

After the treatment, cells or tissues were collected and lysed in RIPA lysis buffer supplemented with Protease Inhibitor Cocktail (Roche, Germany) for 15 min on ice, followed by sonication (Sonics, USA) and centrifugation (Eppendorf, Germany). Then supernatants were collected, and the protein concentration of the samples was measured using the BCA assay (Pierce, USA). After boiling with loading buffer, Proteins (20 μg – 40 μg depending on the target protein) were resolved by 10%-12% SDS-PAGE and transferred to polyvinylidene fluoride (PVDF) membranes (BioRad, USA). The membranes were blocked with 5% non-fat milk for 2 h at RT and subsequently probed with specific primary antibodies overnight at 4°C (Supplementary Table S2). After washing three times with TBST, the membranes were incubated with horseradish peroxidase-conjugated anti-rabbit or anti-mouse IgG for 2 h at room temperature. Then, immunoreactive bands were visualized with an enhanced chemiluminescent substrate according to the manufacturer's protocol (Pierce). The bands were collected using GeneGnomeXRQ (Syngene, UK) and analyzed using the ImageJ 3.5 software. The expression levels of target proteins were determined and

normalized to the housekeeping β-Actin. All Western blot data were presented in samples from at least 3 independent experiments.

Sphere-formation assay

Patient-derived GSCs were infected with lentivirus containing shUTX (KD-UTX) or negative control vectors (shNC). The blank control group (Ctrl) received an equal volume of culture medium. For sphere diameter measurement, single GSCs were seeded at a density of 3,000 cells/well incubated in the 24-well plates. For sphere counting, cells were incubated at a seed density of 6,000 cells/well in the 24-well plates. The sphere diameter and number were) were recorded by using an inverted microscope (Olympus CKX41, Japan) on the 3rd, 5th, and 7th day (inoculation in the 24-well plates was deemed as 0 day). The images were analyzed with ImageJ software, and all spheres per well ≥ 30 μm diameter were included in the count

Animal experiments

Pathogen-free male athymic BALB/c nude mice (5 weeks old) weighing 20-25 g were used for this study and all mouse experiments were approved by the Xi'an Jiaotong University Health Science Center Ethics Committee. The mice were purchased from the Xi'an Jiaotong University Laboratory Animal Center (Certificate No. 22-9601018). The staff at Xi'an Jiaotong University Laboratory Animal Center was responsible for housing and daily maintenance. Housing and environmental enrichment are according to standards. All efforts were undertaken to minimize the suffering of the mice.

For the heterotopic xenograft model, 100 μL of normal LN229 (Blank), sh-NC-LN229 (shNC) or KD-UTX-LN229 (KD-UTX) suspension (1×10^7 / mL) were implanted into the subcutis of the mice. Tumors were monitored every weekday and size was measured by using an electronic digital caliper. If the tumor size exceeds 2000 mm^3 or the diameter exceeds 15 mm, the mice will be weeded out and euthanatized. Five mice were sacrificed at 3 d, 7 d, 14 d, and 28 d respectively. At each time point, tumors were isolated and tumor weight was measured, and tumor size was calculated by the formula: length × width2 × 0.52 [23]. Subsequently, heterotopic tumor tissues were collected and used for Western blot analysis.

For the orthotopic glioma model, mice were anesthetized with inhalational anesthesia using 4% isoflurane for induction and 1.5% isoflurane for maintenance. Then, mice were placed in a stereotactic frame (RWD LifeScience, China) and a longitudinal incision in the cranium was made at the midline to expose the bregma. After drilling a small hole, stably transfected patient-derived GSCs which express luciferase (1×10^5/μL) were implanted into the right brain using the following coordinates: anterior-posterior, -1.3 mm posterior to the bregma; medial-lateral, 1.7 mm; dorsal-ventral, 2.2 mm below the skull surface. The Hamilton syringe was performed slowly over a 1-min period at a speed of 5 μL/min. After the injection, the syringe was left in place for 5 min and the hole was sealed with bone wax. Mice were observed daily for signs of ill health. Mice were imaged using the IVIS® Spectrum In Vivo Imaging System (XENOGEN, USA) at day 3, 7 and 14, respectively.

Transwell co-culture analysis

Patient-derived GSCs (8,000 cells/well) with different treatments were seeded onto a 0.4 μm transwell chamber (Millipore). When the cells covered the bottom of the transwell chamber (this typically takes 3 days), normal GSCs (3000 cells/well) and LN229 cells (1500 cells/well) were seeded in the 24-well plate. At the next day, the transwells were discarded and the cells in the 24-well plate were fixed with 4% PFA for 20 min followed by BrdU incorporation and TUNEL assay.

RNA-sequencing (RNA-seq)

Total RNA was extracted using a Trizolreagent kit (Invitrogen) according to the manufacturer's protocol. RNA quality was assessed on an Agilent 2100 Bioanalyzer (Agilent Technologies, Palo Alto, CA, USA) and checked using RNase-free agarose gel electrophoresis. Eukaryotic mRNA was enriched by Oligo(dT) beads, while prokaryotic mRNA was enriched by removing rRNA by Ribo-Zero^{TM} Magnetic Kit (Epicentre, Madison, USA). Then the enriched mRNA was fragmented into short fragments using a fragmentation buffer and reverse transcripted into cDNA with random primers. Second-strand cDNA was synthesized by DNA polymerase I, RNase H, dNTP and buffer. Then the cDNA fragments were purified with QiaQuick PCR extraction kit (Qiagen, The Netherlands), end-repaired, poly(A) added, and ligated to Illumina sequencing adapters. The ligation products were size selected by agarose gel electrophoresis, amplified by PCR and sequenced using Illumina HiSeq2500 by Gene Denovo Biotechnology Co. (Guangzhou, China). Bioinformatic analysis was performed using Omicsmart, a real-time interactive online platform for data analysis (http://www.omicsmart.com).

Quantitative reverse-transcription PCR (qRT-PCR)

Total RNA was isolated from cells using Trizol reagent following the manufacturer's instructions, and 2 μg RNA was reverse transcribed into cDNA using a RevertAid first-strand cDNA synthesis kit (ThermoFisher, USA) supplemented with Oligo(dT)18 and Random Hexamer Primer. qRT-PCR was performed with GoTaq® qPCR Master Mix (Promega, USA) using an iQ5 Real-Time PCR Detection System (BioRad, USA). The primer pairs were synthesized by TaKaRa and displayed in Supplementary Table S3.

Chromatin Immunoprecipitation (ChIP)-qPCR

ChIP was performed as previously described with minor modifications as detailed below [24]. 100 μL single-cell suspensions (2×10^7 / mL) were fixed by 1% formaldehyde for 10 min. Then, glycine solution (final concentration 125 mM) was added and incubated for 5 min. After twice washing with 500 μL ice-cold PBS, 300 μL lysis buffer was added and sonicated for 3 × 30s using VCX 500 (SONICS, USA). The lysate was diluted and incubated in Dynabeads™ Protein A (Invitrogen, USA) which had pre-incubated with 2 μg of H3K27me2/me3 antibody (39435, Active Motif, USA) or IgG (Abcam, UK). The immune complexes were incubated at 4°C, 20 rpm on a Tube Revolver Rotator for 12 hours. Then, the chromatin–antibody–bead complexes were washed 4 times in 100 μL ice-cold RIPA buffer, rinsed with 400 μL ChIP

elution buffer (containing 50 μg RNase A) and incubated at 37 °C at 1,200 rpm on a Thermomixer (Eppendorf, Germany) for 1 h followed by incubating with 2 μL Proteinase K (New England Biolabs, USA) at 65 °C, 4 hours. An input control was processed in parallel. ChIP DNA was purified by phenol-chloroform isoamyl alcohol extraction, ethanol-precipitated and dissolved in 20 μL EB buffer (Qiagen, Germany). Analysis of DNA was performed using qRT-PCR with gene-specific primers (Supplementary Table S4). Recovery of genomic DNA as the percentage input was calculated as the ratio of immunoprecipitate to input.

The enzyme-linked immunosorbent assay (ELISA)

At the end of each time point, the cell culture medium was collected and analyzed using the POSTN, VCAM1 and Pro-Collagen I alpha 1 ELISA kit (R&D Systems) according to the manufacturer's instructions. The absorbance was measured at 450 nm using a multimicroplate spectrophotometer (BioTek). Triplicate parallel wells were examined in all the experiments and the data were presented as the average of at least three independent experiments.

Cell viability assay

Cell viability was evaluated using the Cell Counting Kit-8 (CCK-8; 7sea, Shanghai, China). Cells were grown in 96-well plates at 5,000 cells/well and cultured for 1, 2, 3, 5 and 7 days. At the end of each treatment, 20 μl/well of CCK-8 was added to the media and cells were incubated for 2 hr at 37°C. The absorbance was measured at 490 nm using a multimicroplate spectrophotometer (BioTek, Winooski, VT). Triplicate parallel wells were examined in all the experiments, and the data were collected as the average of at least three independent experiments. The results are presented as the absorbance value.

Statistical Analysis

Statistical analyses were performed using GraphPad Prism 5.0 software. Data were evaluated for normality and homogeneity of variance before comparison. Differences between groups were analyzed using one-way ANOVA, followed by Tukey's post hoc test. The Kolmogorov-Smirnov test was used for normality and homogeneity. The data were shown as mean ± standard deviation, and $P < 0.05$ was considered as a statistically significant difference.

Results

UTX inhibition contributes to GBM repression processes

To explore the effect of UTX on GBM progression, we first examined the differential expression of UTX among low-grade glioma (LGG), GBM and normal brain tissues by using RNA-seq data from TCGA. Compared to the normal group, UTX expression was higher in the GBM and LGG (Fig. 1 A). Moreover, the expression of UTX was negatively correlated with overall survival for GBM and LGG patients (Fig. 1 B). These results suggested that UTX was a risk factor and UTX inhibition might be developed for GBM treatment. To unambiguously define the role of UTX in GBM, the expression of UTX was suppressed by

RNA interference (RNAi). Two human GBM cell lines (LN229 and U251 MG) were transfected with three UTX-target siRNAs (si-UTX-1/2/3). The combined results from RT-PCR and Western blot indicated that si-UTX-1 exerted a higher inhibition efficiency (Fig. S1 A-E). Therefore, the si-UTX-1 sequence was used in the subsequent lentiviral packaging. The lentivirus-transduced cells were selected using puromycin. We found that the vast majority of cells expressed eGFP and the expression of UTX was significantly decreased (Fig. S1 F-J). This lentivirus for UTX inhibition (KD-UTX) was used for further experiments.

The proliferation effect of UTX on GBM cells was verified by BrdU incorporation, cell cycle analysis and colony-forming assay. The results showed that silencing UTX significantly reduced the number of BrdU positive cells (Fig. 1 C, G and Fig. S2 A, E), the proliferation index (PI) (Fig. S2 B, C, G and H) and the colony-forming capacity (Fig. 1 D, H and Fig. S2 D, F). We further analyzed the effect of UTX on the apoptosis of GBM cells. In contrast to its enhanced proliferation effects, silencing UTX significantly enhanced the number of TUNEL-positive cells (Fig. 1 E, I and Fig. S2 I, K) and the rate of apoptosis (Fig. 1 F, J and Fig. S2 J, L).

To further define the effect of UTX on GBM cell proliferation and apoptosis, the UTX knockdown stable LN229 cells were implanted into the subcutis of the athymic nude mice to establish the heterotopic xenograft model. We measured the tumor volumes and weights, and detected the expression of apoptosis-related Caspase-3 and Cyclin D1 at different time points. Tumor volumes and weights were significantly decreased in the LN229-KD-UTX group (Fig. 1 K-M). Furthermore, UTX inhibition increased the ratio of Cleaved-caspase-3 / Pro-caspase-3, while UTX inhibition suppressed CyclinD1 expression (Fig. 1 N-P). Taken together, these data strongly suggested that silencing UTX inhibited cell proliferation and promoted apoptosis in GBM cells.

UTX inhibition reduced proliferation and increased apoptosis of patient-derived GSCs

One of the hallmarks of GBM is tumor heterogeneity, which means GSCs probably contributes to the bioinformatics analysis of data from TCGA. Thus, we further investigate whether UTX function in the regulation of GSCs. At first, patient-derived GSCs (GSC-02, GSC-05 and GSC-08) were isolated from three post-surgical patients (Fig. 2 A). After culturing 5-7 days, 90-280 μM spheres were formed (Fig. 2 B). The double immunofluorescent staining showed that these spheres expressed cancer stem cell markers, including CD133, CD15, CD44 and nestin (Fig. 2 D, E). Moreover, the single-GSCs staining showed 96.89% ± 5.37% nestin-positive cells, of which 96.65% ± 4.28% expressed SOX2 (Fig. 2 C). These phenomena suggested that these cultured cells were human GSCs, and these patient-derived cells were used for the subsequent experiments.

To measure the effect of UTX on patient-derived GSCs, we suppressed UTX expression by transduction with lentivirus expression shRNA (KD-UTX). Western blot showed that KD-UTX lentivirus could also significantly decrease UTX expression in the patient-derived GSCs (Fig. S3 A, B). Sphere-formation and CCK-8 assay showed that UTX inhibition significantly decreased the number (Fig. 3 A-C), the mean diameter of tumorsphere (Fig. 3 D-F) and cell viability (Fig. 3 G-I). Subsequently, proliferating cells were identified by BrdU incorporation and apoptotic cells were detected by TUNEL staining. Compared to the

shNC group, silencing UTX decreased the number of BrdU-positive cells (Fig. 3 J, K). In contrast, the number of TUNEL-positive cells was significantly increased in the KD-UTX group (Fig. 3 L, M). To further pinpoint the potential role of UTX in cell proliferation and apoptosis, we performed in vivo analyses using a patient-derived GSCs orthotopic glioma mouse model. KD-UTX GSCs or shNC GSCs were implanted into the nude mice, and the fluorescence intensity in tumor tissues was detected by using small animal imaging system at various time points. At the end of the experiment, brain tissues were harvested, and the sections were made. H&E staining showed orthotopic tumor formation by patient-derived GSCs (Fig. 3 O). More importantly, tumor growth was significantly suppressed by UTX inhibition (Fig. 3 N). Collectively, these results suggested that UTX inhibition suppressed proliferation and tumor progression, and promoted apoptosis of patient-derived GSCs.

UTX-regulated gene is closely related to cell proliferation and extracellular microenvironment

To understand the molecular insight by which UTX exerts its effects, total GSCs-02 (the best condition among three patient-derived GSCs) cell RNA was extracted and subjected to differential RNA-sequencing after UTX inhibition treatment. Correlation heatmap showing an exhibited reproducibility (Fig. 4 A) and 568 genes expression were significantly altered by UTX withdrawal. Of these, 446 genes expression increased, while 122 genes decreased (Fig. 4 B). Geneset enrichment analysis (GSEA) showed that the UTX-regulated genes were strongly related with DNA replication, cell cycle regulation and extracellular matrix organization (Fig. 4 C-H). Moreover, Gene Ontology (GO) enrichment (Fig. 4 I), KEGG databases (Fig. 4 J) and Disease Ontology (DO) analysis (Fig. 4 K) indicated that UTX-regulated genes were involved in secretion, extracellular structure organization, intercellular communication and cancer. Collectively, these results suggested that UTX was closely correlated with GBM progression and regulatory TME.

UTX inhibition suppresses many extracellular matrix proteins expression

UTX is linked with the demethylation of lysine residues on H3K27. To validate that UTX regulates the level of H3K27me2/3 in GBM cells, we performed Western blot. As expected, the level of H3K27me2/3 was significantly increased in the KD-UTX group (Fig. 5 A, B). Because H3K27me2/3 is strongly associated with gene repression, the 122 downregulated genes might be directly regulated by UTX inhibition. The top 20 downregulated genes were selected (Fig. 5 C), and qRT-PCR was carried out to validate the sequencing results. Subsequently, the H3K27me2/3 modification level of genes, which were indeed significantly regulated, were further examined by ChIP-qPCR. Among the 20 genes, 17 genes were significantly downregulated (Fig. 5 D) and the levels of H3K27me2/3 were decreased in 13 genes (Fig. 5 E). Interestingly, many genes, including POSTN, VCAM1, SCG5, COL1A1 and ITGBL1, are the major component of the interstitial extracellular matrix. In order to further define the effect of UTX, the expression of extracellular matrix protein and intracellular protein were detected by Western blot and ELISA, respectively. As we expected, UTX inhibition significantly repressed the intracellular protein expressions of COL1A1, VCAM1 and POSTN (Fig. 5 F-K) and decreased their concentrations in the culture medium (Fig. 5 L-N). These above results suggested that UTX was involved in the regulation of the TME.

UTX regulates the proliferation and apoptosis in patient-derived GSCs and GBM cells by changing the TME

Based on the above results, we speculated that UTX-regulated cell behaviors may be by changing the TME. To mimic the changes of the tumor microenvironment, we used normal, shNC or UTX inhibition GSCs transwell co-cultured with normal GSCs and GBM cells, to observe changes in cell proliferation and apoptosis. Specifically, normal, shNC or UTX inhibition GSCs were seeded on the transwell chamber, respectively. Normal GSCs (Fig. 6 A) and LN229 cells (Fig. 6 F) were seeded in the well after cell covering the bottom the transwell chamber. One day later, proliferation and apoptosis were evaluated for changes in the number of BrdU and TUNEL-positive cells in the well plate, respectively. BrdU incorporation assay showed that silencing UTX in the transwell chamber GSCs significantly decreased the number of BrdU-positive GSCs (Fig. 6 B, C) and LN229 cells (Fig. 6 G, H) in the well plate. However, TUNEL-positive cells in the well plate were not observably altered by UTX inhibition (Fig. 6 D, E, I and J). These phenomena suggested that UTX inhibition affected GSCs and GBM cell proliferation mainly by changing the TME.

UTX influences the proliferation and apoptosis of patient-derived GSCs by regulating POSTN expression

Although the above results showed that UTX is strongly associated with the regulation of cellular processes including cell proliferation and apoptosis, by altering the TME. It remains largely unknown what UTX directly regulates the key target gene. To identify the master regulator, the proteins, which are regulated by H3K27me2/3, were analyzed by the STRING database to reveal the protein-protein interaction networks (PPI) and figured out the hub proteins in the network. The result showed that the POSTN protein could interact with many extracellular matrix proteins (Fig. 7 A, B). Moreover, silencing UTX inhibited the expression of POSTN protein (Fig. S3 C, D) and mRNA (Fig. S3 E) in cultured patient-derived GSCs, while enhancing the H3K27me2/3 levels in the POSTN gene (Fig. S3 F). Thus, it is reasonable to assume that POSTN plays a pivotal role in the UTX-mediated transcriptional regulatory network. To clarify whether POSTN participated in UTX-mediated regulation of cell proliferation and apoptosis, 2 μg/mL recombinant human POSTN protein was replenished in the KD-UTX cell culture medium, the proliferation and apoptosis of patient-derived GSCs were measured by BrdU incorporation and TUNEL staining, respectively. Similar to our previous results, UTX inhibition significantly decreased the number of SOX2 BrdU double-positive cells. Interestingly, supplement POSTN protein abolished the effect of UTX inhibition on cell proliferation (Fig. 7 C-E, G). Further TUNEL staining indicated that positive cells were also increased in the KD-UTX group, and supplement POSTN protein eliminated the pro-apoptotic effect of UTX inhibition (Fig. 7 F, H). Moreover, we also examined the change in the expression of COL1A1 and VCAM1 (both of them could interact with POSTN). The ELISA assay indicated that UTX inhibition decreased extracellular concentrations of COL1A1 and VCAM1, and this difference was notably ablated in the POSTN replenishment group (Fig. 8 A, B). Similar results were obtained with ELISA, western blot analysis showed that the intracellular concentrations of COL1A1 and VCAM1 were also decreased after silencing UTX, while supplement POSTN blocked the effect of UTX inhibition (Fig. 8 C-E). The above results suggested the importance of POSTN played a key role in UTX-mediated proliferation and apoptosis of patient-derived GSCs.

Discussion

In this study, we showed that UTX expression was much higher in the GBM and LGG, and negatively correlated with overall survival. Under normal conditions, patient-derived GSCs displays high proliferative capability and low rate of apoptosis because of the existence of sufficient UTX. When inhibiting UTX expression, H3K27 methylation in the POSTN is promoted, thereby suppressing POSTN expression. The low expression level of POSTN repressed lots of extracellular matrix proteins expression (including COL1A1, COL3A1 and VCAM1) that would impact on the TME, which in turn inhibits proliferation and promotes apoptosis (Fig. 9). These results suggested that UTX was an oncogenic factor and could promote growth and tumorigenesis, and UTX inhibitor might consider as a novel therapeutic target for rational GBM drug development. However, targeting UTX for cancer treatment remains controversial. Although prior reports have demonstrated that UTX plays a pro-oncogenic role [25], some have reported the role of UTX as a tumor suppressor [26, 27]. We found a large difference in UTX expression in different tumor types (Fig. S4 A, B). This large difference may, in part, be responsible for the differences in the effect of UTX among different cancer types. Another reason may be that UTX is a subunit of MLL3 and MLL4, which are members of the COMPASS family of histone H3 lysine 4 (H3K4) methyltransferases [28]. Compared to the UTX, H3K4 methylation has the opposite effect on the regulation of gene expression [29]. H3K4 methylation is tightly associated with transcriptional start sites of actively transcribed genes [30]. The biological role of UTX and MLL3/MLL4 in cancer pathogenesis is quite complicated. The mechanistic relationship between UTX and MLL3/MLL4 and their regulation of enhancer activity, whether local or global is still unclear. Our results showed that silencing UTX in GSCs just affected 568 genes expression, perhaps indicating that UTX and MLL3/MLL4 just influence local genomic features. Further studies are necessary to understand the fundamental mechanism and precise functional impact of MLL3/MLL4 and UTX alterations.

The TME is a dynamic network structure and has emerged as a key factor to regulate tumor occurrence, development, invasion and recurrence [31, 32]. Therefore, anticancer research cannot be just understood the features of cancer cells, but instead should encompass the effect of the TME [33]. In this study, the results of RNA-seq, ELISA and western blot assay showed that UTX inhibition modulated many secretions and extracellular structure organization-related genes expression. These altered genes (like POSTN, COL1A1, and VCAM1) have been critically linked to tumor development and progression [34–36]. More importantly, the transwell co-cultured experiment revealed that silencing UTX inhibited cell proliferation mainly by changing the TME. However, no significant effect of UTX inhibition was observed on apoptosis. One possible reason for this phenomenon is the presence of normal GSCs or GBM cells in the culture system. Cells in both the transwell chamber and the well plate together constituted the TME. Even though UTX inhibition reduced the extracellular matrix proteins expression and secretion from GSCs in the transwell chamber, the normal GSCs or GBM cells in the well plate could partially complement extracellular matrix proteins deficiency, which might lead to eliminate the pro-apoptotic effect of UTX inhibition.

As one of the matricellular proteins, POSTN is mainly secreted by stromal cells in normal tissues. But tumor cells, especially cancer stem cells, can also secret POSTN in solid tumors [37]. POSTN has played a vital role in regulating tumor progression and tumorigenesis through remodeling various tumor microenvironments, such as cancer stem cell niche, perivascular niche, and immunosuppressive microenvironment [38–41]. In this study, PPI analysis showed that POSTN protein could interact with many extracellular matrix proteins which regulated by UTX. And POSTN replenishment could eliminate the effect of UTX inhibition on the proliferation and apoptosis in GSCs and recover to the previous level of COL1A1and VCAM1. These results strongly suggested that POSTN was a key regulator of the antitumor effect of UTX inhibition. Moreover, compared to the GSCs which sorting from cell lines, the patient-derived GSCs represent a more realistic response in terms of recapitulating the individual differences [42]. In this study, we used patient-derived GSCs to examine UTX functions, and this enhances the trustworthiness of our findings. However, the effect of UTX cannot simply account for the inhibition of POSTN expression. Many other tumor-associated proteins like COL1A1, ENC1, VCAM1 and ITGBL1 were also regulated by UTX, we cannot rule out the effect of these proteins. Whether these proteins mediate the antitumor mechanism remains to be seen.

The tumorigenesis and progression of GBM constitute a very complex process, both genetic and epigenetic alterations are involved [43]. Because alterations of histone methylation are reversible, drugs targeting these processes have a broad clinical application prospect in treating GBM [44]. In this study, we demonstrated that UTX inhibition could enhance the H3K27me2/3 level in the POSTN gene, which inhibited the expression of many extracellular matrix proteins including POSTN, eventually resulting in altering the proliferation and apoptosis of patient-derived GSCs. These results reported here enriched the effect of UTX in the regulatory mechanism of tumorigenesis and development, and may also provide a novel and effective strategy for the treatment of GBM. However, additional research, especially studying about resistance, is necessary for an in-depth understanding of the precise mechanisms of UTX in GSCs.

Declarations

Acknowledgements

The authors are grateful to Dr. Jia Wang, Dr. Zhenyu Guo and Dr Xingyu Miao for providing the technical support to carry out this work.

Author contributions

Zhichao Zhang designed the experiments. Xinlin Chen, Haixia Lu, Zhichao Zhang, and Yong Liu supervised the research. Jingwen Xue and Ke Wang performed animal breeding. Yuan Luan and Yingfei Liu performed most of the other experiments. Zhichao Zhang prepared manuscript drafts. Kaige Ma and Yong Liu edited the paper.

Funding

This work was supported by grants from National Natural Science Foundation of China (No. 81901156, 82001493, 82271200); the Fundamental Research Funds for the Central Universities (xzy012022035).

Data availability

The data used and/or analyzed during the current study are available from the corresponding author on reasonable request.

Conflict of interest

No potential conflicts of interest are disclosed.

Ethical approval

Clinical information and samples were obtained with informed consent. Patient-derived cell culture and all mouse experiments were approved by the Xi'an Jiaotong University Health Science Center Ethics Committee (No. 2021-1607). This study conforms to the Declaration of Helsinki.

References

1. Davis ME. Glioblastoma: Overview of Disease and Treatment. Clin J Oncol Nurs. 2016;20(5 Suppl):S2-8. doi: 10.1188/16.CJON.S1.2-8.
2. Shergalis A, Bankhead A, 3rd, Luesakul U, Muangsin N, Neamati N. Current Challenges and Opportunities in Treating Glioblastoma. Pharmacol Rev. 2018;70(3):412-45. doi: 10.1124/pr.117.014944.
3. Tang C, Ang BT, Pervaiz S. Cancer stem cell: target for anti-cancer therapy. FASEB J. 2007;21(14):3777-85. doi: 10.1096/fj.07-8560rev.
4. Dirkse A, Golebiewska A, Buder T, Nazarov PV, Muller A, Poovathingal S, et al. Stem cell-associated heterogeneity in Glioblastoma results from intrinsic tumor plasticity shaped by the microenvironment. Nat Commun. 2019;10(1):1787. doi: 10.1038/s41467-019-09853-z.
5. Shpargel KB, Sengoku T, Yokoyama S, Magnuson T. UTX and UTY demonstrate histone demethylase-independent function in mouse embryonic development. PLoS Genet. 2012;8(9):e1002964. doi: 10.1371/journal.pgen.1002964.
6. Mansour AA, Gafni O, Weinberger L, Zviran A, Ayyash M, Rais Y, et al. The H3K27 demethylase Utx regulates somatic and germ cell epigenetic reprogramming. Nature. 2012;488(7411):409-13. doi: 10.1038/nature11272.
7. Shpargel KB, Starmer J, Wang C, Ge K, Magnuson T. UTX-guided neural crest function underlies craniofacial features of Kabuki syndrome. Proc Natl Acad Sci U S A. 2017;114(43):E9046-E55. doi: 10.1073/pnas.1705011114.
8. Van der Meulen J, Speleman F, Van Vlierberghe P. The H3K27me3 demethylase UTX in normal development and disease. Epigenetics. 2014;9(5):658-68. doi: 10.4161/epi.28298.

9. Tran N, Broun A, Ge K. Lysine Demethylase KDM6A in Differentiation, Development, and Cancer. Mol Cell Biol. 2020;40(20). doi: 10.1128/MCB.00341-20.
10. Kobatake K, Ikeda KI, Nakata Y, Yamasaki N, Ueda T, Kanai A, et al. Kdm6a Deficiency Activates Inflammatory Pathways, Promotes M2 Macrophage Polarization, and Causes Bladder Cancer in Cooperation with p53 Dysfunction. Clin Cancer Res. 2020;26(8):2065-79. doi: 10.1158/1078-0432.CCR-19-2230.
11. Lu H, Xie Y, Tran L, Lan J, Yang Y, Murugan NL, et al. Chemotherapy-induced S100A10 recruits KDM6A to facilitate OCT4-mediated breast cancer stemness. J Clin Invest. 2020;130(9):4607-23. doi: 10.1172/JCI138577.
12. Ji G, Zhou W, Du J, Zhou J, Wu D, Zhao M, et al. PCGF1 promotes epigenetic activation of stemness markers and colorectal cancer stem cell enrichment. Cell Death Dis. 2021;12(7):633. doi: 10.1038/s41419-021-03914-2.
13. Sui A, Xu Y, Li Y, Hu Q, Wang Z, Zhang H, et al. The pharmacological role of histone demethylase JMJD3 inhibitor GSK-J4 on glioma cells. Oncotarget. 2017;8(40):68591-8. doi: 10.18632/oncotarget.19793.
14. Plaks V, Kong N, Werb Z. The cancer stem cell niche: how essential is the niche in regulating stemness of tumor cells? Cell Stem Cell. 2015;16(3):225-38. doi: 10.1016/j.stem.2015.02.015.
15. Liu Y, Huang Z, Cui D, Ouyang G. The Multiaspect Functions of Periostin in Tumor Progression. Adv Exp Med Biol. 2019;1132:125-36. doi: 10.1007/978-981-13-6657-4_13.
16. Cui D, Huang Z, Liu Y, Ouyang G. The multifaceted role of periostin in priming the tumor microenvironments for tumor progression. Cell Mol Life Sci. 2017;74(23):4287-91. doi: 10.1007/s00018-017-2646-2.
17. Malanchi I, Santamaria-Martinez A, Susanto E, Peng H, Lehr HA, Delaloye JF, et al. Interactions between cancer stem cells and their niche govern metastatic colonization. Nature. 2011;481(7379):85-9. doi: 10.1038/nature10694.
18. Ma H, Wang J, Zhao X, Wu T, Huang Z, Chen D, et al. Periostin Promotes Colorectal Tumorigenesis through Integrin-FAK-Src Pathway-Mediated YAP/TAZ Activation. Cell Rep. 2020;30(3):793-806 e6. doi: 10.1016/j.celrep.2019.12.075.
19. Squadrito ML, De Palma M. A niche role for periostin and macrophages in glioblastoma. Nat Cell Biol. 2015;17(2):107-9. doi: 10.1038/ncb3095.
20. Mikheev AM, Mikheeva SA, Trister AD, Tokita MJ, Emerson SN, Parada CA, et al. Periostin is a novel therapeutic target that predicts and regulates glioma malignancy. Neuro Oncol. 2015;17(3):372-82. doi: 10.1093/neuonc/nou161.
21. Zhou W, Ke SQ, Huang Z, Flavahan W, Fang X, Paul J, et al. Periostin secreted by glioblastoma stem cells recruits M2 tumour-associated macrophages and promotes malignant growth. Nat Cell Biol. 2015;17(2):170-82. doi: 10.1038/ncb3090.
22. Azari H, Millette S, Ansari S, Rahman M, Deleyrolle LP, Reynolds BA. Isolation and Expansion of Human Glioblastoma Multiforme Tumor Cells Using the Neurosphere Assay. Jove-J Vis Exp.

2011(56). doi: ARTN e3633 10.3791/3633.

23. Tomayko MM, Reynolds CP. Determination of subcutaneous tumor size in athymic (nude) mice. Cancer Chemother Pharmacol. 1989;24(3):148-54. doi: 10.1007/BF00300234.
24. Lim DA, Huang YC, Swigut T, Mirick AL, Garcia-Verdugo JM, Wysocka J, et al. Chromatin remodelling factor Mll1 is essential for neurogenesis from postnatal neural stem cells. Nature. 2009;458(7237):529-33. doi: 10.1038/nature07726.
25. Kaneko S, Li X. X chromosome protects against bladder cancer in females via a KDM6A-dependent epigenetic mechanism. Sci Adv. 2018;4(6):eaar5598. doi: 10.1126/sciadv.aar5598.
26. Ntziachristos P, Tsirigos A, Welstead GG, Trimarchi T, Bakogianni S, Xu L, et al. Contrasting roles of histone 3 lysine 27 demethylases in acute lymphoblastic leukaemia. Nature. 2014;514(7523):513-7. doi: 10.1038/nature13605.
27. Xie G, Liu X, Zhang Y, Li W, Liu S, Chen Z, et al. UTX promotes hormonally responsive breast carcinogenesis through feed-forward transcription regulation with estrogen receptor. Oncogene. 2017;36(39):5497-511. doi: 10.1038/onc.2017.157.
28. Sze CC, Shilatifard A. MLL3/MLL4/COMPASS Family on Epigenetic Regulation of Enhancer Function and Cancer. Cold Spring Harb Perspect Med. 2016;6(11). doi: 10.1101/cshperspect.a026427.
29. Zaidi S, Choi M, Wakimoto H, Ma L, Jiang J, Overton JD, et al. De novo mutations in histone-modifying genes in congenital heart disease. Nature. 2013;498(7453):220-3. doi: 10.1038/nature12141.
30. Shilatifard A. The COMPASS family of histone H3K4 methylases: mechanisms of regulation in development and disease pathogenesis. Annu Rev Biochem. 2012;81:65-95. doi: 10.1146/annurev-biochem-051710-134100.
31. Ribeiro Franco PI, Rodrigues AP, de Menezes LB, Pacheco Miguel M. Tumor microenvironment components: Allies of cancer progression. Pathol Res Pract. 2020;216(1):152729. doi: 10.1016/j.prp.2019.152729.
32. Wang Q, Hu B, Hu X, Kim H, Squatrito M, Scarpace L, et al. Tumor Evolution of Glioma-Intrinsic Gene Expression Subtypes Associates with Immunological Changes in the Microenvironment. Cancer Cell. 2017;32(1):42-56 e6. doi: 10.1016/j.ccell.2017.06.003.
33. Panigrahi DP, Praharaj PP, Bhol CS, Mahapatra KK, Patra S, Behera BP, et al. The emerging, multifaceted role of mitophagy in cancer and cancer therapeutics. Semin Cancer Biol. 2020;66:45-58. doi: 10.1016/j.semcancer.2019.07.015.
34. Yamauchi M, Barker TH, Gibbons DL, Kurie JM. The fibrotic tumor stroma. J Clin Invest. 2018;128(1):16-25. doi: 10.1172/JCI93554.
35. Kong DH, Kim YK, Kim MR, Jang JH, Lee S. Emerging Roles of Vascular Cell Adhesion Molecule-1 (VCAM-1) in Immunological Disorders and Cancer. Int J Mol Sci. 2018;19(4). doi: 10.3390/ijms19041057.
36. Li X, Sun X, Kan C, Chen B, Qu N, Hou N, et al. COL1A1: A novel oncogenic gene and therapeutic target in malignancies. Pathol Res Pract. 2022;236:154013. doi: 10.1016/j.prp.2022.154013.

37. Liu YF, Huang ZJ, Cui D, Ouyang GL. The Multiaspect Functions of Periostin in Tumor Progression. Periostin. 2019;1132:125-36. doi: 10.1007/978-981-13-6657-4_13.
38. Gonzalez-Gonzalez L, Alonso J. Periostin: A Matricellular Protein With Multiple Functions in Cancer Development and Progression. Front Oncol. 2018;8:225. doi: 10.3389/fonc.2018.00225.
39. Masuoka M, Shiraishi H, Ohta S, Suzuki S, Arima K, Aoki S, et al. Periostin promotes chronic allergic inflammation in response to Th2 cytokines. J Clin Invest. 2012;122(7):2590-600. doi: 10.1172/JCI58978.
40. Zhou WC, Ke SQ, Huang Z, Flavahan W, Fang XG, Paul J, et al. Periostin secreted by glioblastoma stem cells recruits M2 tumour-associated macrophages and promotes malignant growth. Nature Cell Biology. 2015;17(2):170-+. doi: 10.1038/ncb3090.
41. Ghajar CM, Peinado H, Mori H, Matei IR, Evason KJ, Brazier H, et al. The perivascular niche regulates breast tumour dormancy. Nature Cell Biology. 2013;15(7):807-+. doi: 10.1038/ncb2767.
42. Nagle PW, Plukker JTM, Muijs CT, van Luijk P, Coppes RP. Patient-derived tumor organoids for prediction of cancer treatment response. Seminars in Cancer Biology. 2018;53:258-64. doi: 10.1016/j.semcancer.2018.06.005.
43. Thompson JA, Christensen BC, Marsit CJ. Pan-Cancer Analysis Reveals Differential Susceptibility of Bidirectional Gene Promoters to DNA Methylation, Somatic Mutations, and Copy Number Alterations. Int J Mol Sci. 2018;19(8). doi: 10.3390/ijms19082296.
44. Bennett RL, Licht JD. Targeting Epigenetics in Cancer. Annu Rev Pharmacol Toxicol. 2018;58:187-207. doi: 10.1146/annurev-pharmtox-010716-105106.

Figures

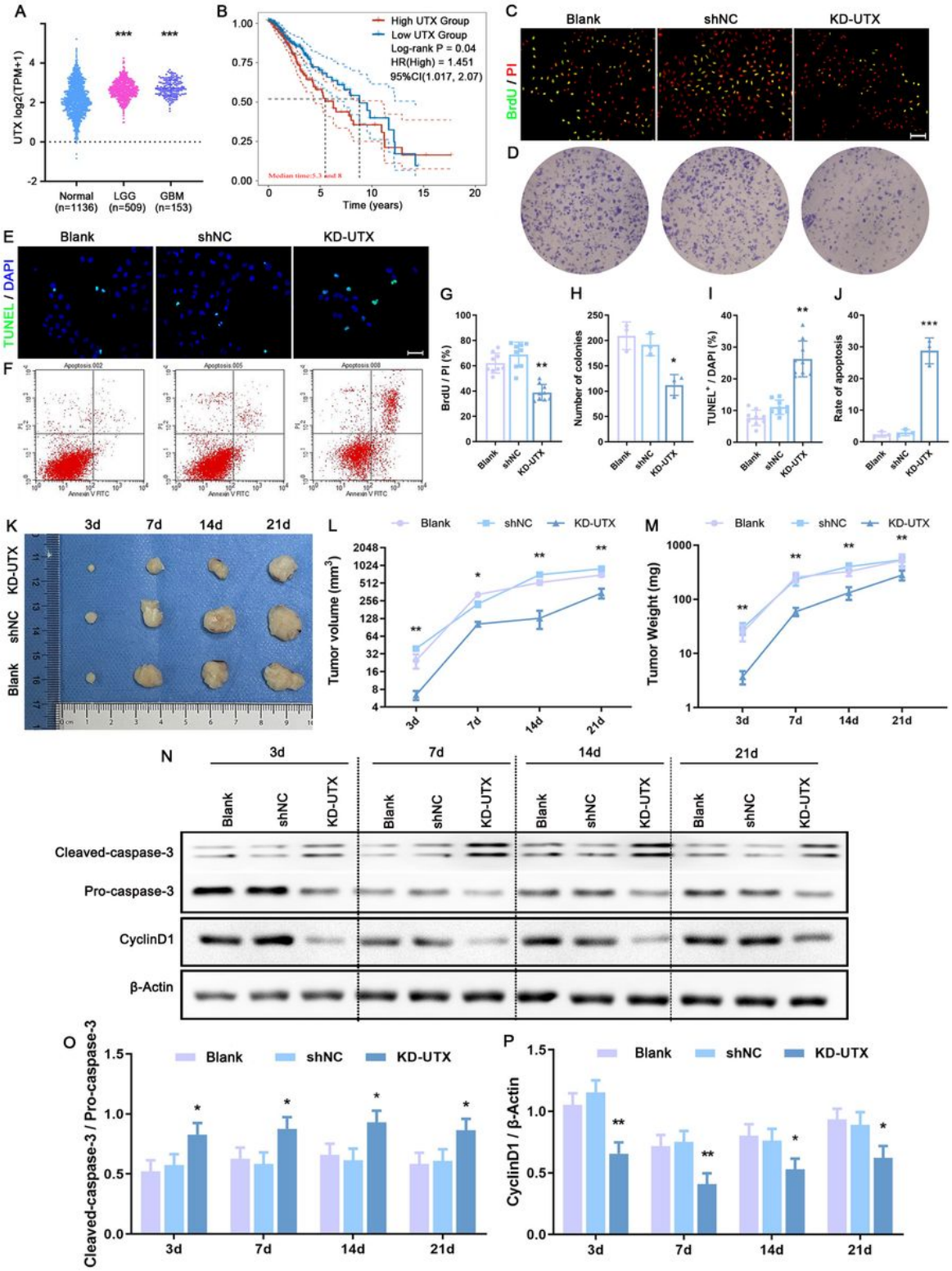

Figure 1

UTX inhibition influences the proliferation and apoptosis of GBM cells.

(A) The expression distribution of the UTX gene among GBM (n=153), LGG (n=509) and normal tissues. ***$p < 0.001$ versus the normal group. (B) Kaplan-Meier survival analysis of the glioma patients with lower and higher levels of UTX from the TCGA dataset. LN229 cells were divided into three groups. Blank

group: cells were maintained without any treatment; shNC group: cells infected with lentiviruses carrying negative control (shNC); KD-UTX group: cells infected with lentiviruses carrying UTX-target shRNA (KD-UTX). (C, G) After culturing 3 days, BrdU-positive cells were determined by immunostaining, and the result was shown as percentages among PI-stained cells. Scale bar = 100 μm. Data are presented as the mean ± standard deviation of nine independent experiments (n = 9). $^{**}p < 0.01$ versus the shNC group. (D, H) A colony formation assay was performed to assess cell colony-forming ability. Data are presented as the mean ± standard deviation of three independent experiments (n = 3). $^{*}p < 0.05$ versus the shNC group. After culturing 3 days, TUNEL staining (E) and flow cytometry analysis (F) were performed to evaluate cell apoptosis. Scale bar = 50 μm. (I) Data are presented as the mean ± standard deviation of nine independent experiments (n = 9). $^{**}p < 0.01$ versus the shNC group. (J) Data are presented as the mean ± standard deviation of three independent experiments (n = 3). $^{***}p < 0.001$ versus the shNC group. The UTX knockdown stable LN229 cells (1×10^6 per injection) were implanted subcutaneously into the nude mice to build the xenograft model. As a negative control, shNC LN229 cells (1×10^6 per injection) were implanted subcutaneously into the nude mice. For Blank control, 1×10^6 of normal LN229 cells were implanted subcutaneously into the nude mice. Mice were killed at 3, 7, 14, and 28 days (the third day after cell inoculation was deemed as 0 d). Five mice of each group were killed at each timepoint, tumors were removed for photograph (K), the measure of the tumor volumes (L) and weights (M), and Western blotting (N). Band intensity was quantified and plotted as a ratio of Cleaved-caspase-3 to Pro-caspase-3 (O) and Cyclin D1 to β-Actin (P). Data are presented as the mean ± standard deviation of three independent experiments (n = 3). $^{*}p < 0.05$, $^{**}p < 0.01$ versus the shNC group. LGG, Low-grade glioma; GBM, glioblastoma.

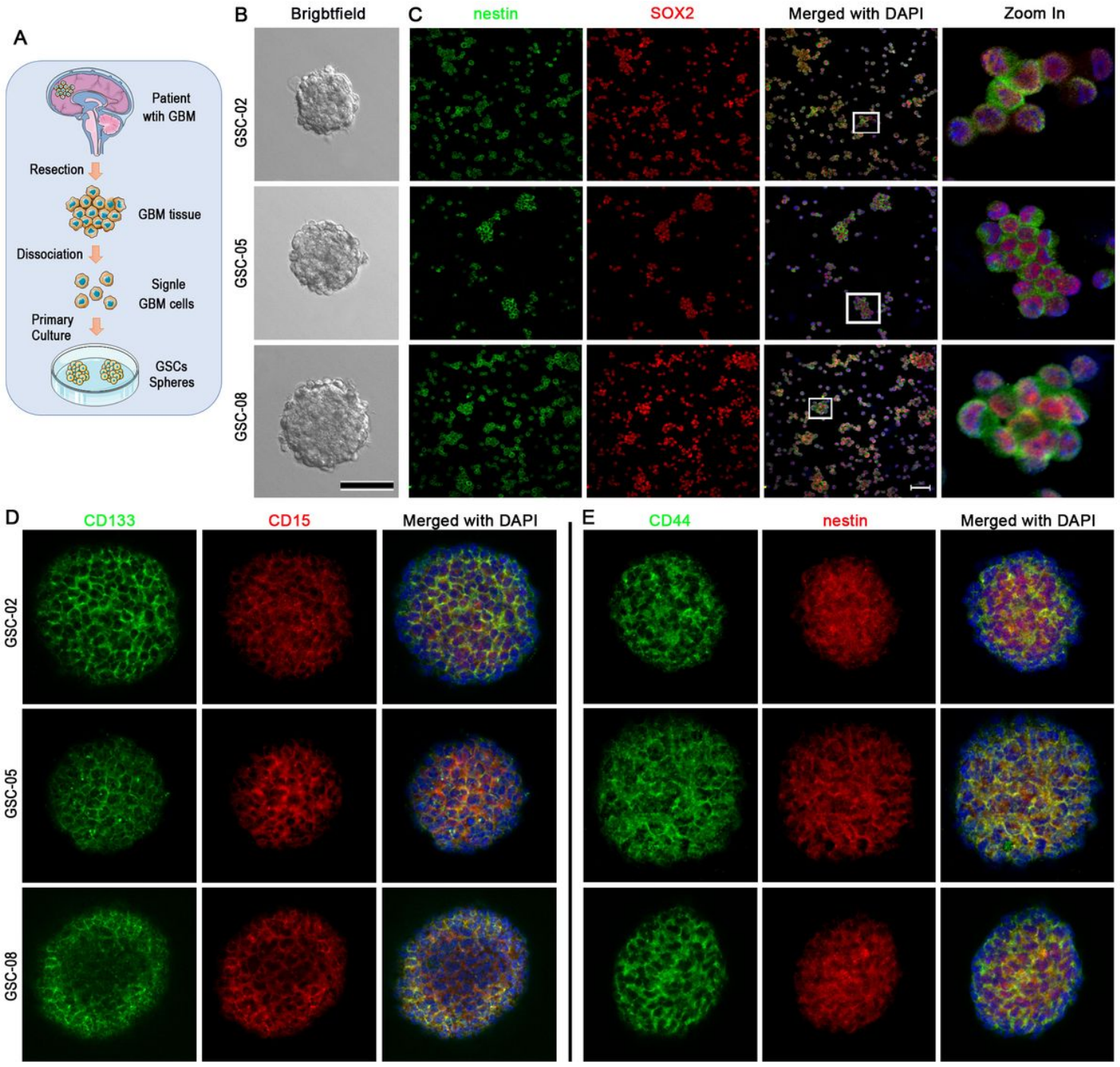

Figure 2

Culture and immunostaining characterization of patient-derived GSCs.

(A) Flow diagram of isolation and culture of patient-derived GSCs. Human GSCs were isolated from three post-surgical patients (GSC-02, GSC-05, and GSC-08). (B) After culturing for 5-7 days, 80-200 μm tumorspheres were observed. Scale bar = 200 μm. (C) SOX2 and nestin double-positive cells are detected in the single GSCs. Scale bar = 50 μm. The right panel represents magnified pictures of square frames in the corresponding left panel. The spheres were identified by double immunofluorescent labeling for specific markers CD133 and CD15 (D) or CD44 and nestin (E).

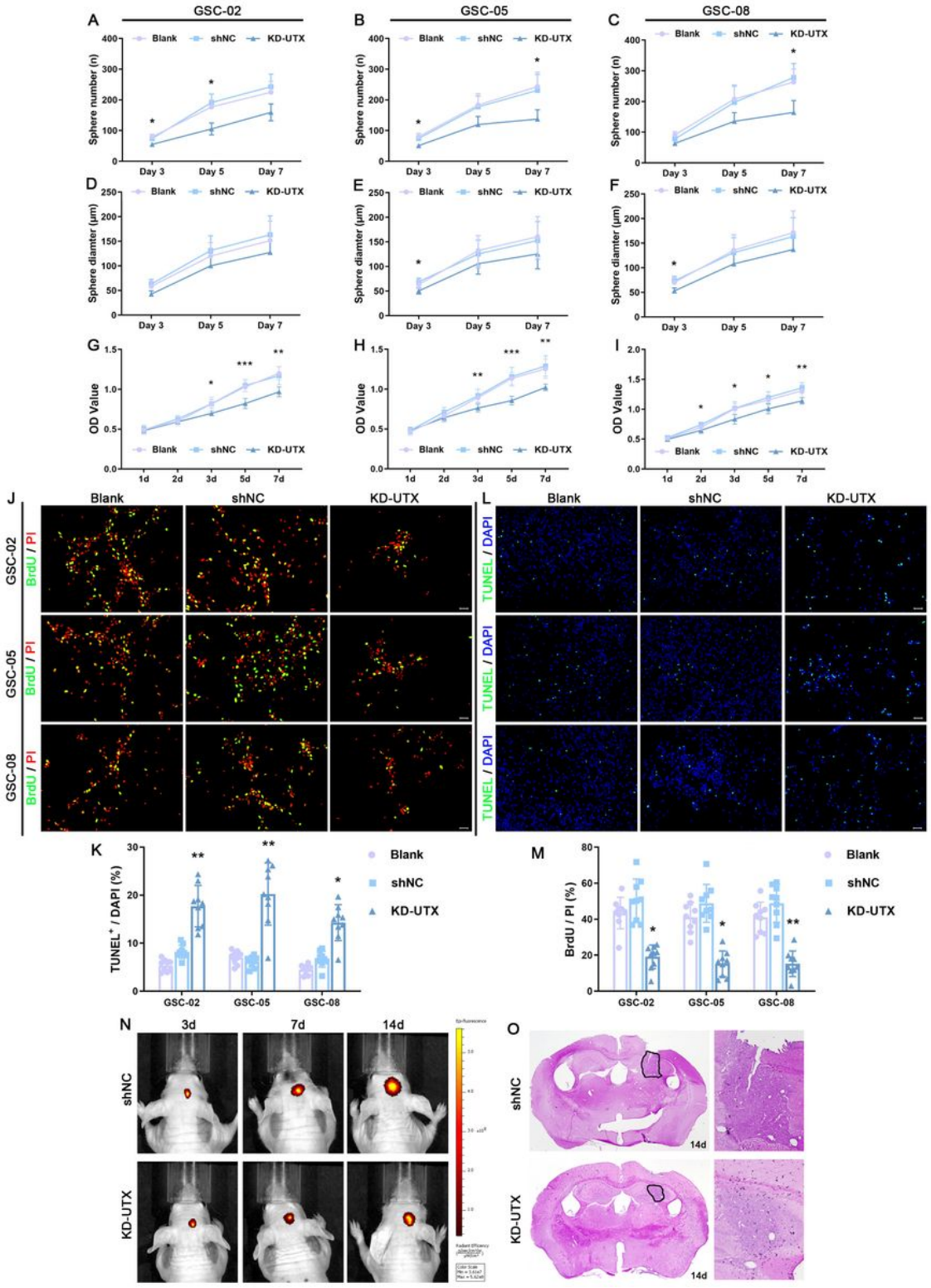

Figure 3

UTX inhibition suppresses cell proliferation and promotes apoptosis of patient-derived GSCs.

Three patient-derived GSCs (GSC-02, GSC-05, and GSC-08) were divided into three groups. Blank group: cells were maintained without any treatment; shNC group: cells infected with lentiviruses carrying negative control (shNC); KD-UTX group: cells infected with lentiviruses carrying UTX-target shRNA (KD-

UTX). After transfection treatment, the sphere number (A-C), the mean diameter (D-F) and cell viability (G-I) were measured at different time points. Data are presented as the mean ± standard deviation of three independent experiments (n = 3). *$p < 0.05$, **$p < 0.01$, ***$p < 0.001$ versus shNC group. Cell proliferation was identified by BrdU incorporation (J) and apoptotic cells were detected by TUNEL staining (L). (K, M) Data are presented as the mean ± standard deviation of nine independent experiments (n = 9). *$p < 0.05$, **$p < 0.01$ versus shNC group. Scale bar, 50 μm (J), 100 μm (L). The luciferase-expressing shNC GSCs or KD-UTX GSCs were used to establish the orthotopic glioma mouse model. (N) The in vivo imaging of shNC GSCs and KD-UTX GSCs in tumor bearing mice at different time points after injection. (O) At the end of the experiment, H&E staining showed orthotopic tumor formation.

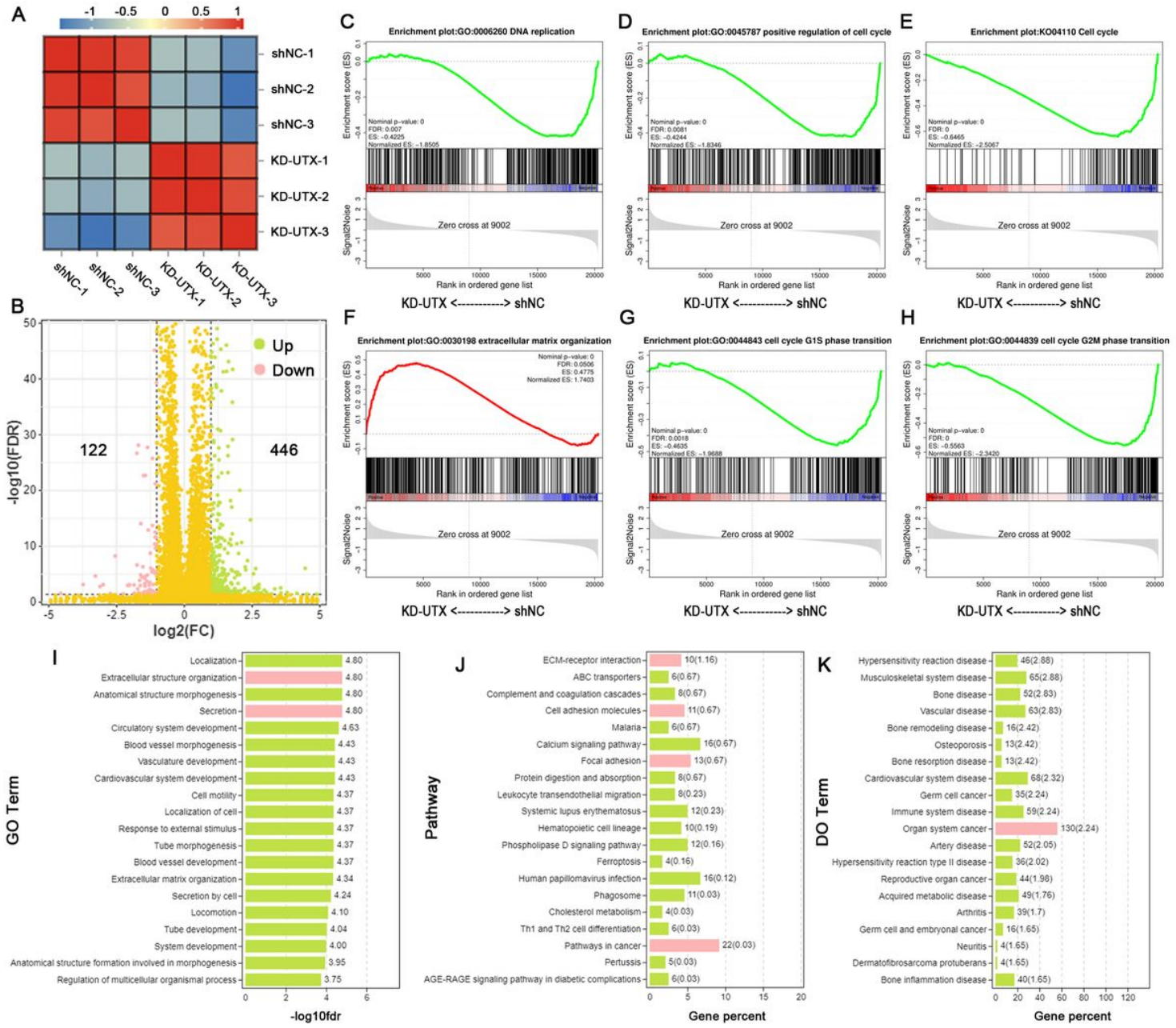

Figure 4

UTX is robustly associated with the regulation of proliferation and extracellular matrix proteins expression

After culturing 3 days, whole-transcriptome sequencing (RNA-seq) was performed for the UTX knockdown stablepatient-derived GSCs (KD-UTX) and cells transfected with scramble shRNA (shNC). (A) Heatmap of the inter-individual correlation of all mRNA transcripts (RNA-seq). (B) Volcano plots showed global differences between the shNC and KD-UTX group. GSEAenrichment plot (C-H), GO enrichment analysis (I), KEGG signaling pathway analysis (J) and DO enrichment analysis (K) were used to analyze the RNA-seq results. GSEA, gene-set enrichment analysis; GO, gene ontology; DO, disease ontology; KEGG, Kyoto Encyclopedia of Genes and Genomes.

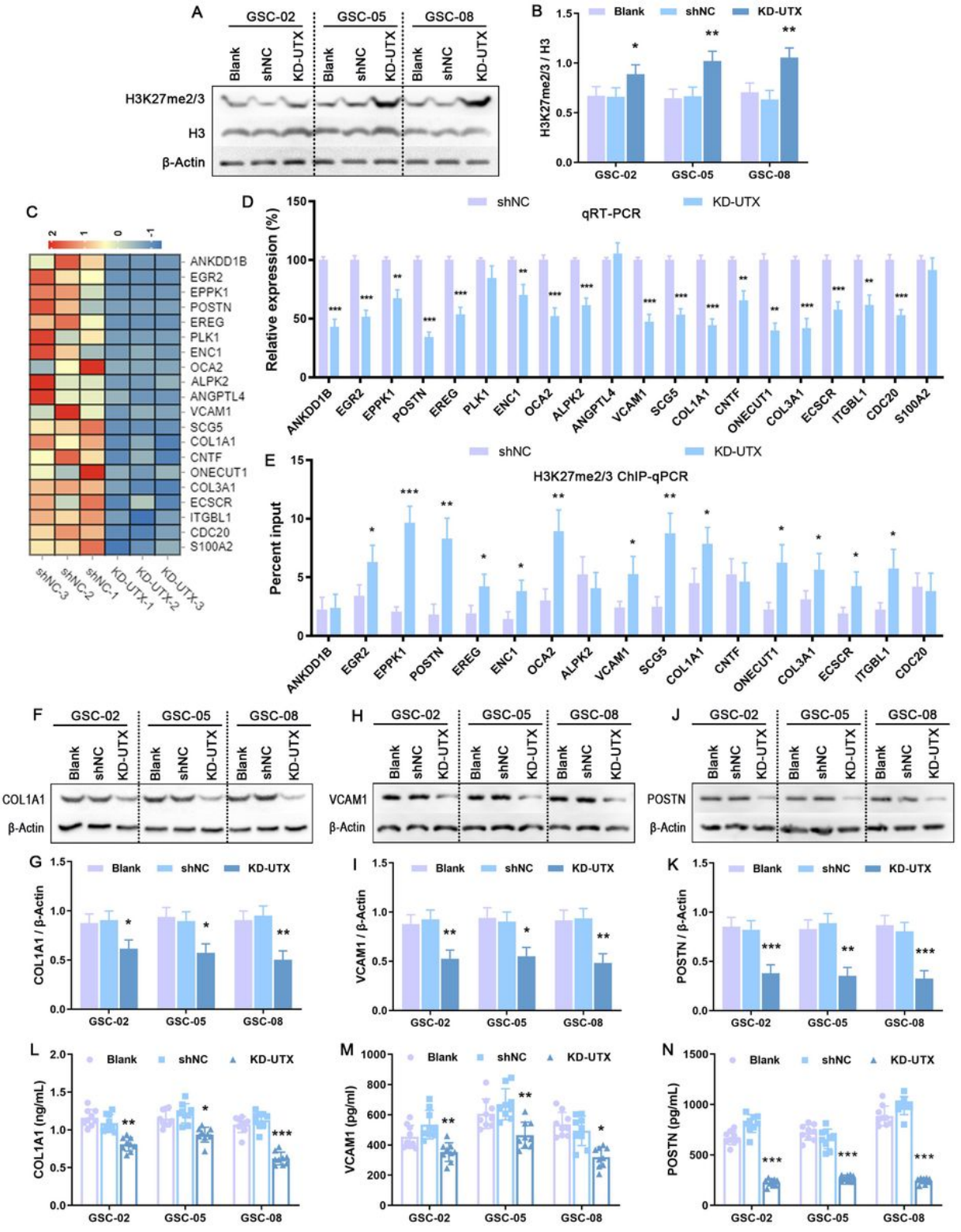

Figure 5

UTX inhibition suppresses the expression of extracellular matrix-related genes via enhancing the levels of H3K27 methylation.

(A, B) After culturing 3 days, the cells were lysed and total protein was harvested. The level of H3K27me2/3 and histone H3 were detected by Western blot. Data from three independent experiments (n

= 3) were presented as the ratio of H3K27me2/3 to H3. The values are presented as the mean ± standard deviation of three independent experiments (n = 3). *$p < 0.05$, **$p < 0.01$ versus shNC group. The heat map shows the top 20 downregulated genes in knockdown UTX GSCs in comparison to shNC GSCs (C), and the 20 downregulated genes were validated by qRT-PCR (D). (E) ChIP-qPCR was used to measure the H3K27me2/3 enrichment in the significantly downregulated genes. The values are presented as the mean ± standard deviation of three independent experiments (n = 3). *$p < 0.05$, **$p < 0.01$, ***$p < 0.001$ versus shNC group. (F-K) The intracellular protein expressions of COL1A1, VCAM1 and POSTN were examined by Western blot. Band intensity was quantified and plotted as a ratio of the target protein to β-Actin. The values are presented as the mean ± standard deviation of three independent experiments (n = 3). *$p < 0.05$, **$p < 0.01$, ***$p < 0.001$ versus shNC group. COL1A1 (L), VCAM1 (M) and POSTN (N) concentrations in the culture medium were detected by ELISA. The values are presented as the mean ± standard deviation of nine independent experiments (n = 9). *$p < 0.05$, **$p < 0.01$, ***$p < 0.001$ versus shNC group.

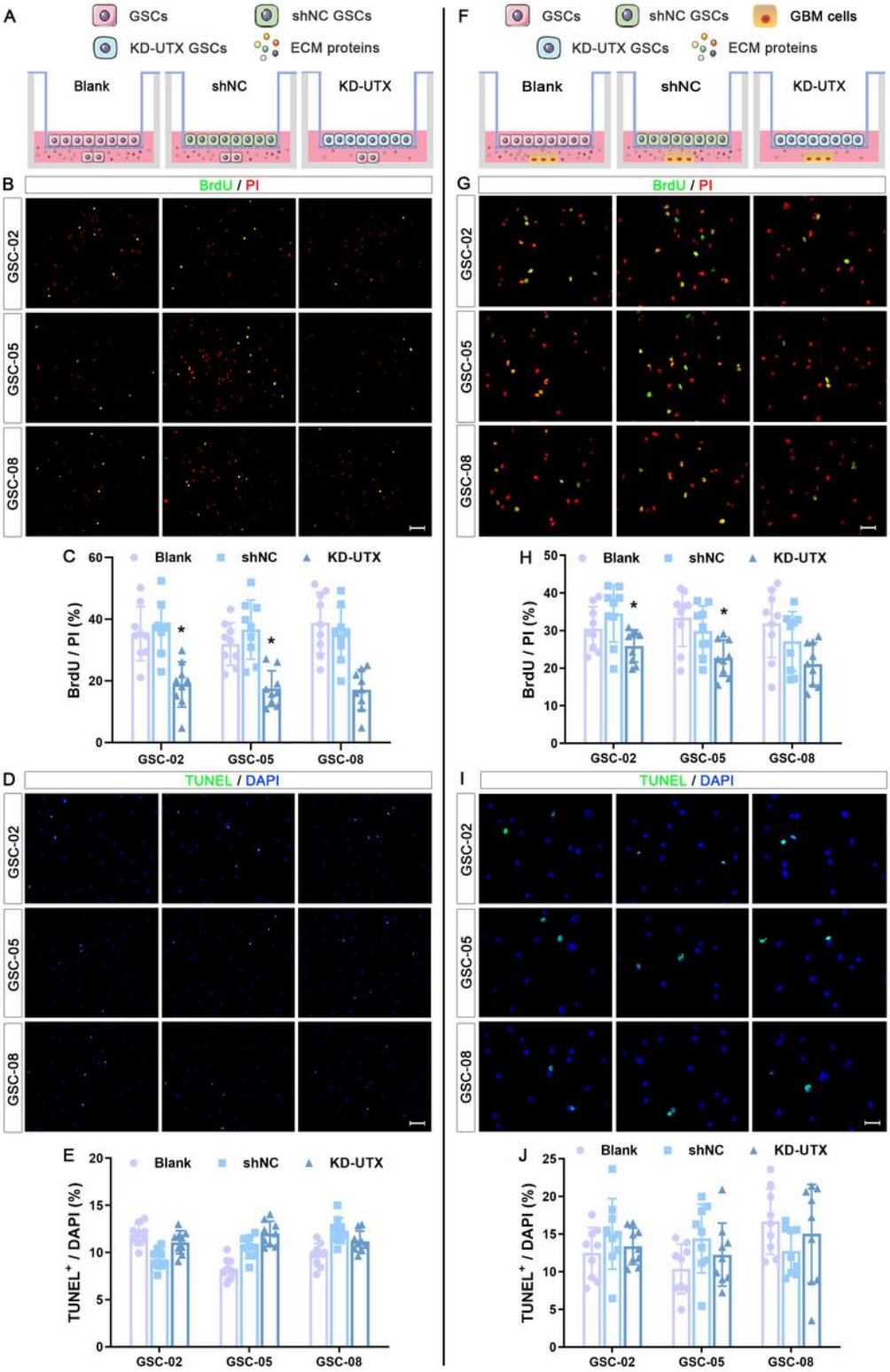

Figure 6

UTX affects cell proliferation and apoptosis by the tumor microenvironment

Diagram of the transwell co-culture experiment. After transfection, patient-derived GSCs was seeded onto a 0.4 μm transwell chamber. When the cells covered the bottom of the transwell chamber,normal GSCs (A) or LN299 (F) were seeded in the 24-well plate. At the next day, the proliferation of GSCs (B) or LN299

(G) in the 24-well plate was identified by BrdU incorporation. The apoptosis of GSCs (D) or LN299 (I) in the 24-well plate were detected by TUNEL staining. (C, E, H and J) Data are presented as the mean ± standard deviation of nine independent experiments (n = 9). *p< 0.05 versus the shNC group. Scale bar, 100 μm (B, C), 50 μm (G, I).

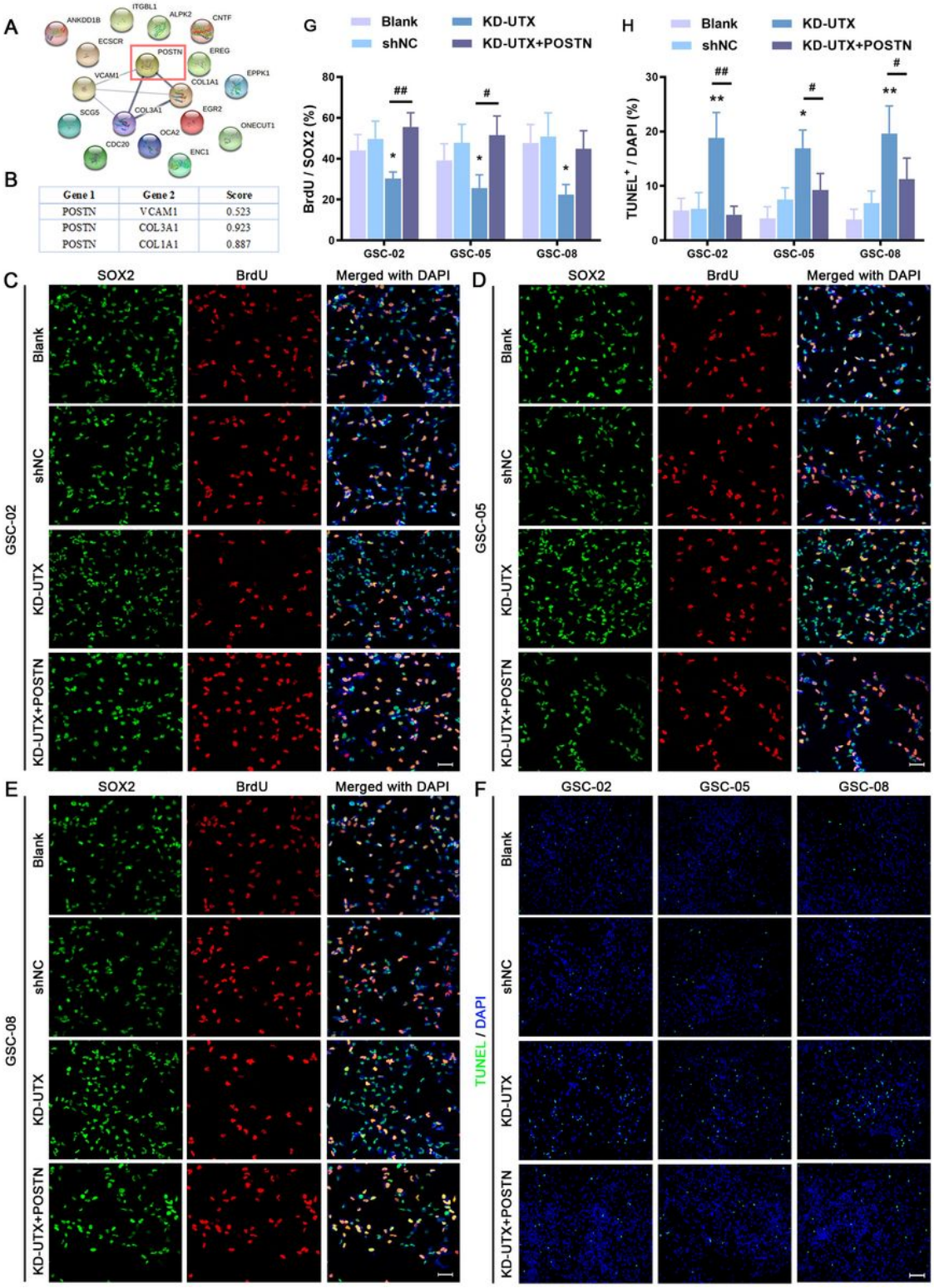

Figure 7

POSTN replenishment abolishes the effect of UTX inhibition on cell proliferation and apoptosis of patient-derived GSCs

(A) UTX-regulated proteins were screened for protein interactions (grey lines, the confidence score ≥ 0.4) by using the STRING database, and the interaction score between POSTN and other proteins were shown (B). Three patient-derived GSCs (GSC-02, GSC-05, and GSC-08) were divided into four groups. Blank group: cells were maintained without any treatment; shNC group: cells infected with lentiviruses carrying negative control (shNC); KD-UTX group: cells infected with lentiviruses carrying UTX-target shRNA (KD-UTX); KD-UTX +POSTN group: cells infected with KD-UTX followed by POSTN (2 μg/mL) treatment. After culturing 3 days, cell proliferation was identified by BrdU incorporation (C-E) and apoptotic cells were detected by TUNEL staining (F). (G) Quantitative data from nine independent experiments (n = 9) were shown as the percentage of BrdU-positive cells in total SOX2-positive cells. (H) Quantitative data from nine independent experiments (n = 9) are presented as the percentage of TUNEL-positive cells in the total DAPI cells. *$p < 0.05$, **$p < 0.01$ versus shNC group; $^{\#}P < 0.05$, $^{\#\#}P < 0.01$ versus KD-UTX group. Scale bar, 50 μm (C-E), 100 μm (F).

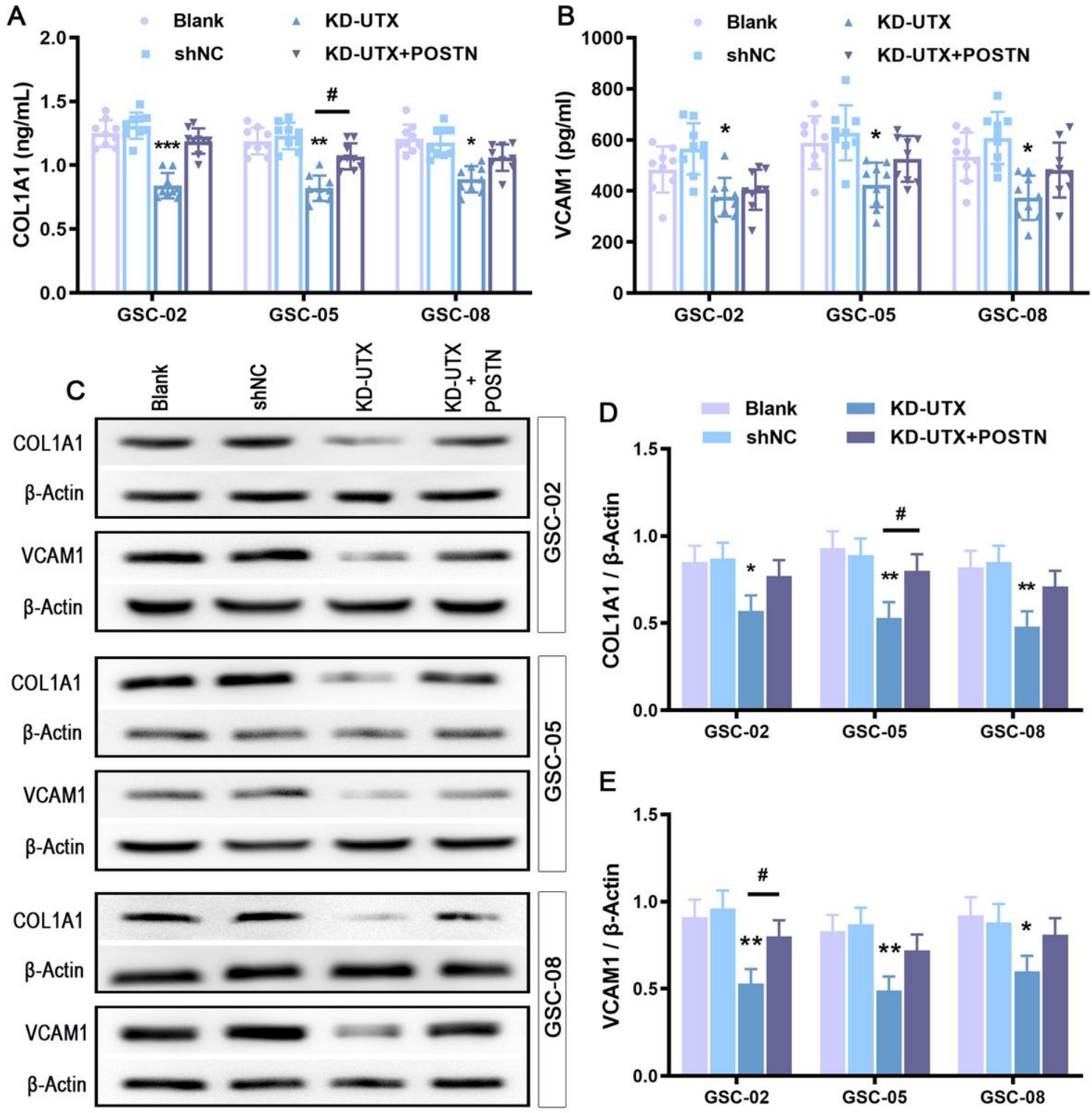

Figure 8

POSTN replenishment eliminates the effect of UTX inhibition on the expression of COL1A1 and VCAM1

Three patient-derived GSCs (GSC-02, GSC-05, and GSC-08) were treated as above for 3 days. (A, B) Extracellular concentrations of COL1A1 and VCAM1 were measured by ELISA assay. The values are presented as the mean ± standard deviation of nine independent experiments (n = 9). *$p < 0.05$, **$p < 0.01$, ***$p < 0.001$ versus shNC group; $^{\#}P < 0.05$ versus KD-UTX group. (C-E) Intracellular concentrations of

COL1A1 and VCAM1 were detected by Western blot. Band intensity was quantified and plotted as a ratio of the target protein to β-Actin. The values are presented as the mean ± standard deviation of three independent experiments (n = 3). *$p < 0.05$, **$p < 0.01$ versus shNC group; $^{\#}P < 0.05$ versus KD-UTX group.

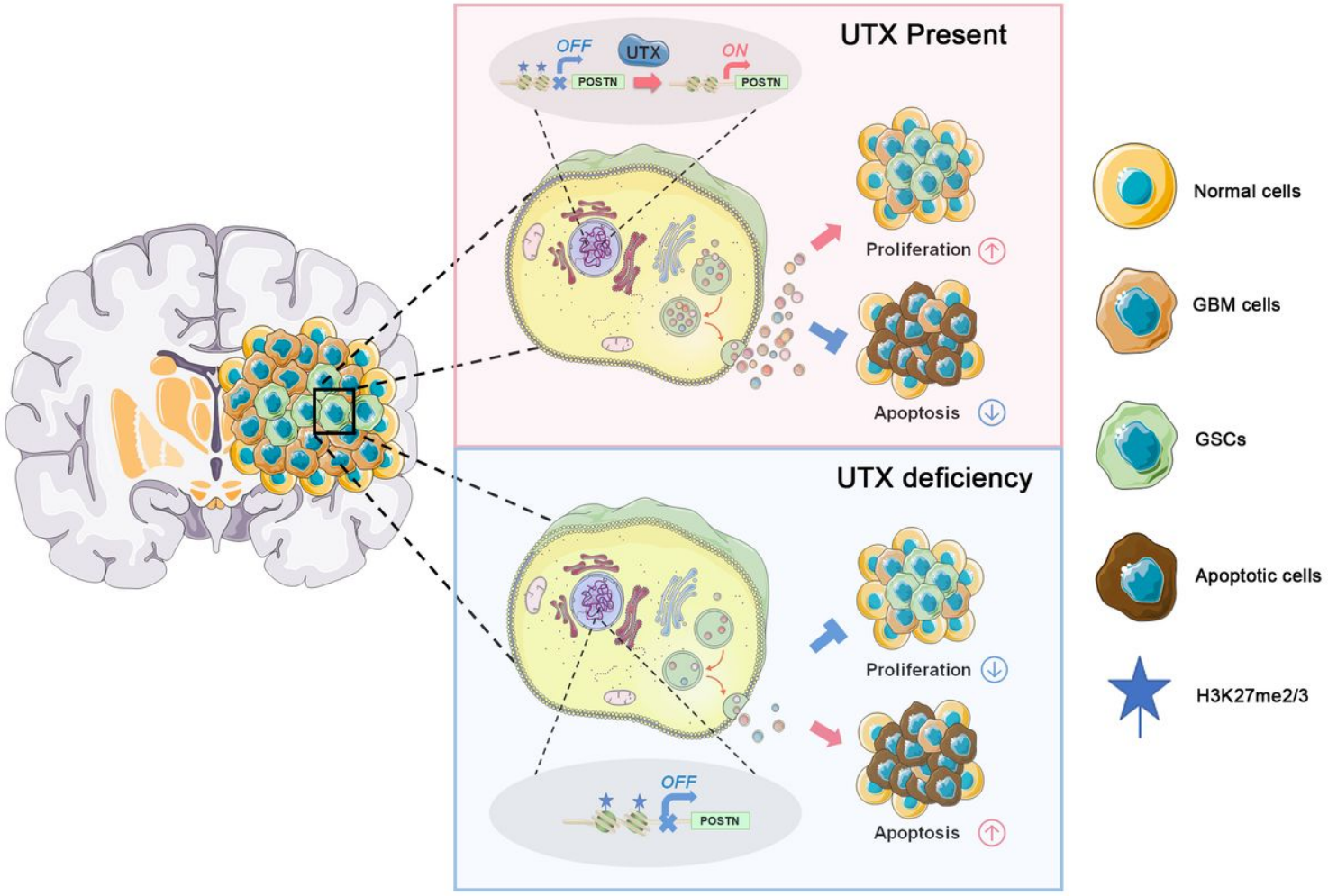

Figure 9

Illustration depicts the mechanism by which UTX inhibition regulates the proliferation and apoptosis of patient-derived GSCs.

The expression level of UTX is significantly increased in GSCs (up panel) and results in a low H3K27me2/3 level in the POSTN gene that culminates with activated transcription. POSTN protein can interact with lots of secreted proteins. These proteins, the important components of the tumor microenvironment, are involved in the regulation of proliferation and apoptosis of GSCs. UTX inhibition (down panel) significantly increases the H3K27me2/3 level in the POSTN gene, which in turn represses the transcription of POSTN. Fewer proteins, especially interaction with POSTN, are secreted to the extracellular matrix and change the tumor microenvironment, thereby inhibiting proliferation and promoting apoptosis.

Supplementary Files

This is a list of supplementary files associated with this preprint. Click to download.

- Fig.S1.jpg
- Fig.S2.jpg
- Fig.S3.jpg
- SupplementaryFigurelegend.docx
- SupplementaryTableS1PatientandTumorCharacteristics.docx
- SupplementaryTableS2Antibodiesusedduringthestudy.docx
- SupplementaryTableS3PCRprimer.doc
- SupplementaryTableS4chippcrprimer.docx